3-2014

On the cause and extent of outer radiation belt losses during the 30 September 2012 dropout event

D. L. Turner
University of California - Los Angeles

V. Angelopoulos
University of California - Los Angeles

S. K. Morley
Los Alamos National Laboratory

M. G. Henderson
Los Alamos National Laboratory

Geoffrey Reeves
Los Alamos National Laboratory

See next page for additional authors

Recommended Citation
Turner, D. L., et al. (2014), On the cause and extent of outer radiation belt losses during the 30 September 2012 dropout event, J. Geophys. Res. Space Physics, 119, 1530–1540, doi:10.1002/2013JA019446

AGU PUBLICATIONS

JGR

Journal of Geophysical Research: Space Physics

BRIEF REPORT

10.1002/2013JA019446

Key Points:
- Dropout events can encompass the entire outer radiation belt
- Dropouts can result in >90% losses and be a hard reset on the system
- Loss at $L > \sim 4$ is dominated by MP shadowing and outward transport

Supporting Information:
- Readme
- Text S1

Correspondence to:
D. L. Turner,
drew.lawson.turner@gmail.com

Citation:
Turner, D. L., et al. (2014), On the cause and extent of outer radiation belt losses during the 30 September 2012 dropout event, *J. Geophys. Res. Space Physics*, *119*, 1530–1540, doi:10.1002/2013JA019446.

Received 12 SEP 2013
Accepted 18 FEB 2014
Accepted article online 24 FEB 2014
Published online 17 MAR 2014

On the cause and extent of outer radiation belt losses during the 30 September 2012 dropout event

D. L. Turner[1], V. Angelopoulos[1], S. K. Morley[2], M. G. Henderson[2], G. D. Reeves[2], W. Li[3], D. N. Baker[4], C.-L. Huang[5], A. Boyd[5], H. E. Spence[5], S. G. Claudepierre[6], J. B. Blake[6], and J. V. Rodriguez[7]

[1]Department of Earth, Planetary, and Space Sciences, University of California, Los Angeles, California, USA, [2]Space Sciences and Applications, Los Alamos National Laboratory, Los Alamos, New Mexico, USA, [3]Department of Atmospheric and Oceanic Sciences, University of California, Los Angeles, California, USA, [4]Laboratory for Atmospheric and Space Physics, University of Colorado Boulder, Boulder, Colorado, USA, [5]Institute for the Study of Earth, Oceans, and Space, University of New Hampshire, Durham, New Hampshire, USA, [6]The Aerospace Corporation, El Segundo, California, USA, [7]Cooperative Institute for Research in Environmental Sciences, University of Colorado Boulder, Boulder, Colorado, USA

Abstract On 30 September 2012, a flux "dropout" occurred throughout Earth's outer electron radiation belt during the main phase of a strong geomagnetic storm. Using eight spacecraft from NASA's Time History of Events and Macroscale Interactions during Substorms (THEMIS) and Van Allen Probes missions and NOAA's Geostationary Operational Environmental Satellites constellation, we examined the full extent and timescales of the dropout based on particle energy, equatorial pitch angle, radial distance, and species. We calculated phase space densities of relativistic electrons, in adiabatic invariant coordinates, which revealed that loss processes during the dropout were >90% effective throughout the majority of the outer belt and the plasmapause played a key role in limiting the spatial extent of the dropout. THEMIS and the Van Allen Probes observed telltale signatures of loss due to magnetopause shadowing and subsequent outward radial transport, including similar loss of energetic ring current ions. However, Van Allen Probes observations suggest that another loss process played a role for multi-MeV electrons at lower L shells ($L^* < \sim 4$).

1. Introduction

Flux "dropout" events have been observed to occur regularly in Earth's outer electron radiation belt. Dropouts involve the drastic decrease in relativistic electron flux over a broad range in energy, equatorial pitch angle, and radial distance in only a few hours, as observed by spacecraft, and the dominant mechanism(s) responsible for these events remains a topic of debate. Based on some of the earliest observations of outer belt electrons, *Dessler and Karplus* [1961] presented a theory that explained dropouts as simply an adiabatic effect during the main phase of geomagnetic storms: essentially, as the magnetic field strength in the inner magnetosphere dropped during storm main phase, electron drift shells expanded in physical space to conserve the third adiabatic invariant, Φ or L^* [*Roederer*, 1970], and as the particles moved away from the Earth to regions of lower field strength, they lost energy due to conservation of the first and second adiabatic invariants, μ and K. Since there are exponentially fewer particles at higher energy, this adiabatic motion would be observed as a distinct drop in particle flux. However, it has now been shown that dropouts can also occur independent of geomagnetic storms [e.g., *Morley et al*., 2010] and that the adiabatic effects alone cannot explain the magnitude of loss observed during dropouts [e.g., *Kim and Chan*, 1997; *Li et al*., 1997]. The clearest evidence that outer belt dropouts are driven by true losses from the system (i.e., not just adiabatic effects) have resulted from studies of events, revealing that distributions of electron phase space density (PSD) in adiabatic invariant coordinates, which remove most of the ambiguity due to purely adiabatic effects, also undergo outer belt dropouts [e.g., *Turner et al*., 2013]. Here we use the definition of dropouts described in *Turner et al*. [2012b], which includes both adiabatic effects and nonadiabatic losses.

Currently, it is believed that losses during dropouts are dominated by one, or a combination, of two mechanisms, both of which can act in the presence of adiabatic motion: (i) rapid scattering into the atmospheric loss cones (i.e., either the drift or bounce loss cone) and (ii) magnetopause shadowing and subsequent enhanced outward radial transport. Rapid losses to the atmosphere are believed to occur due to wave-particle interactions between relativistic electrons and electromagnetic ion cyclotron (EMIC) waves [e.g., *Summers and*

Thorne, 2003], possibly within plasmaspheric plumes that form during active periods and span the radial extent of the outer radiation belt [*Borovsky and Denton*, 2009]. Typically, only electrons with energy > ~2 MeV can resonate with EMIC waves [*Meredith et al*., 2003], though during very active conditions this resonant energy limit might decrease to ~400 keV [*Ukhorskiy et al*., 2010]. Scattering rates from EMIC waves also depend on electrons' equatorial pitch angles, with electrons nearest the loss cone being scattered most rapidly [*Shprits et al*., 2008].

Magnetopause shadowing involves the loss of trapped particles on drift trajectories that intersect the magnetopause following sudden compressions of the magnetosphere [e.g., *Kim et al*., 2008]. Losses can extend to L^* lower than those directly affected by the magnetopause shadowing due to a rapid cascade of outward radial transport that can occur if the distinct PSD radial distribution remaining after magnetopause shadowing is perturbed by wave activity that violates the third invariant [e.g., *Shprits et al*., 2006; *Miyoshi et al*., 2006; *Loto'aniu et al*., 2010; *Turner et al*., 2012a]. However, arguments have been made against this mechanism based on energetic ring current ions not observed to undergo similar behavior concurrently [i.e., *Green et al*., 2004], since magnetopause shadowing and subsequent outward transport should affect trapped energetic ring current ions much like the electrons. Another possibility for dropouts that has yet to be thoroughly investigated is rapid deceleration due to nonlinear wave-particle interactions [e.g., *Tao et al*., 2012], the effects of which should also depend on electron energy and equatorial pitch angle. For additional details on the history and current understanding of outer belt dropouts, see *Turner et al*. [2012b].

We investigated a dropout event that occurred on 30 September to 1 October 2012, which we chose because of the drastic effect it had on the outer belt, including the eradication of the double outer belt structure identified by *Baker et al*. [2013] and the unprecedented level of observational coverage provided by NASA's new Van Allen Probes (formerly Radiation Belt Storm Probes, RBSP) [*Mauk et al*., 2012] and THEMIS [*Angelopoulos*, 2008] missions combined with NOAA's GOES spacecraft at geosynchronous orbit (GEO). With such extensive multipoint coverage, this event allowed us to examine the timescales and full extent of the dropout for different particle energies, equatorial pitch angles, L^*, and species, which we present here. These observations revealed the interesting nature of this dropout and provided strong evidence of the dominant loss mechanisms responsible for the drastic loss of energetic particles throughout Earth's inner magnetosphere.

2. Observations

On 30 September 2012, the solar wind exhibited two sudden increases in dynamic pressure. Figure 1 shows solar wind data from the OMNI data set, which have been propagated to Earth's subsolar bow shock. The two steplike increases in dynamic pressure occurred around 11:20 UT and just after 23:00 UT, and despite both pressure enhancements being associated with sudden increases in the solar wind speed, the solar wind remained slow (i.e., below its average value of ~425 km/s) throughout the entire period. The interplanetary magnetic field (IMF) also demonstrated some drastic variations during this period (Figure 1b). *Bz* went strongly southward for more than 16 h, and the total IMF strength increased to ~8 nT after the first pressure enhancement and up to > 20 nT following the second. These two distinct regions were likely related to an interplanetary coronal mass ejection, based on typical sheath and magnetic cloud signatures [e.g., *Kilpua et al*., 2013] evident in Figure 1, though thorough classification was unnecessary for this study. This activity spawned a strong geomagnetic storm, with a *Dst* minimum of approximately −135 nT around 04:00 UT on 1 October (not shown).

Figure 1 also reveals the orbital configurations for the spacecraft used for this study (Figure 1d) and the time history of the magnetopause standoff distance (based on the *Lin et al*. [2010] model using the OMNI data shown as inputs) and the last closed drift shell of equatorially mirroring electrons in the outer radiation belt, L^*_{max}, from the *Koller and Zaharia* [2011] neural network model (Figure 1c). The two Van Allen Probes spacecraft (referred to hereinafter as RBSP-A and RBSP-B) were in near-identical, ~9 h period orbits in the dawn local time sector with an apogee of ~5.8 R_E. The three THEMIS spacecraft, also each in very similar orbits to each other, had orbital periods of ~23 h and apogees of ~12 R_E in the dusk sector. Both the Van Allen Probes and THEMIS constellations passed through the outer belt in the magnetic equatorial zone multiple times per day.

We examined electron and proton fluxes on the RBSP-Energetic particle, Composition, and Thermal plasma (ECT) instrument suite [*Spence et al*., 2013] from the RBSP-ECT Magnetic Electron and Ion Spectrometers (MagEIS) [*Blake et al*., 2013]. We also calculated electron PSD in adiabatic coordinates using fluxes from the RBSP-ECT Relativistic Electron and Proton Telescopes (REPT) [*Baker et al*., 2012] and THEMIS Solid State Telescopes (SST) [*Angelopoulos*, 2008; *Turner et al*., 2012c]. The THEMIS-SST, RBSP-ECT REPT, and MagEIS

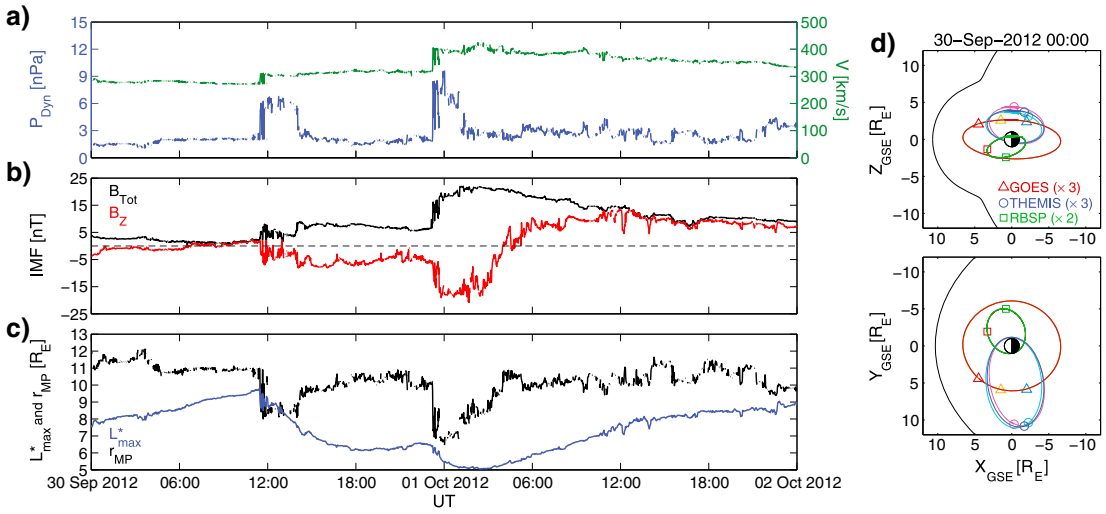

Figure 1. (a, b) Solar wind data from the OMNI data set, including dynamic pressure (P_{Dyn}), speed (V), and IMF strength (B_{Tot}) and Z_{GSE} component (B_Z). (c) The subsolar magnetopause standoff distance from the *Lin et al.* [2010] model and the last closed drift shell (L^*_{max}) from the *Koller and Zaharia* [2011] model; both models were run using OMNI data. (d) Spacecraft orbits for Van Allen Probes (RBSP-A in red and RBSP-B in green orbits with squares), THEMIS (THA in magenta, THD in cyan, and THE in blue orbits with circles), and GOES (GOES-13 in teal, GOES-14 in gold, and GOES-15 in dark red orbits with triangles). Symbols indicate the spacecraft locations at 00:00 UT on 30 September 2012. The *Lin et al.* [2010] magnetopause is also shown from the same time.

instruments all measure the full pitch angle distributions throughout each spin of the spacecraft. To convert to PSD, pitch angle and energy resolved fluxes were fit to energy spectra at each time and converted to PSD as a function of energy by dividing by the corresponding relativistic momentum squared. The first adiabatic invariant, μ, was calculated as a function of electron energy directly using the local magnetic field strengths measured by each spacecraft. All values of the invariants K and L^* were calculated at each measurement point with the *Tsyganenko and Sitnov* [2005] magnetospheric field model (TS05). The array of PSD data as a function of energy, pitch angle, and location was then simply mapped to invariant coordinates (μ, K, and L^*) at each time. For additional details on conversion from fluxes to PSD, see *Turner et al.* [2012c] for THEMIS and *Reeves et al.* [2013] for RBSP-ECT REPT, which used the same methods employed here for each mission's data, respectively. *Turner et al.* [2012c] and *Morley et al.* [2013] also discussed the errors associated with PSD calculated from each of these data sets, which are consistently less than ~20%. Finally, three GOES spacecraft (GOES-13, GOES-14, and GOES-15) were also operating during this event; they spanned ~4 h in local time in their 24 h, ~6.6 R_E orbits.

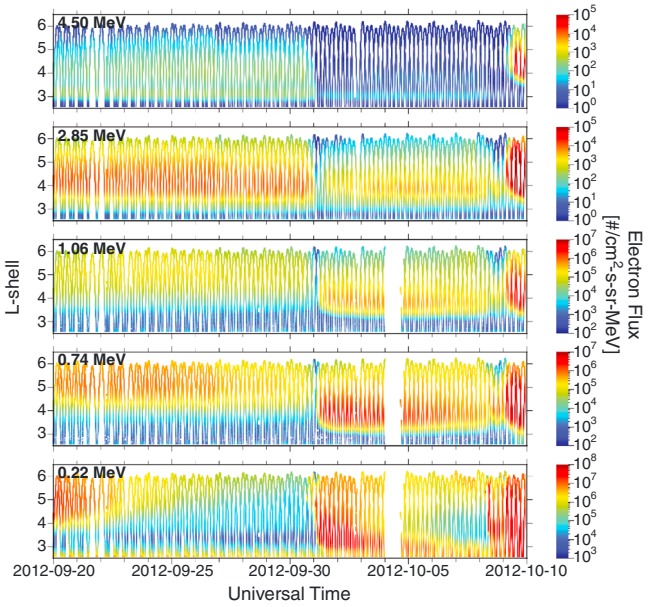

Figure 2. Overview of RBSP-ECT MagEIS and REPT electron differential fluxes from five different energy channels plotted (logarithmic scale in color) versus time and L shell. The energy bin centers for each of the five channels is labeled in bold at the top left of each plot, and note that the color scales are different for several of the channels. The data shown are from both RBSP-A and RBSP-B at spin resolution (~11 s) and have been averaged over all look directions during each spin.

An overview of the outer radiation belt electrons as observed by the Van Allen Probes during the period around the dropout is shown in Figure 2. The

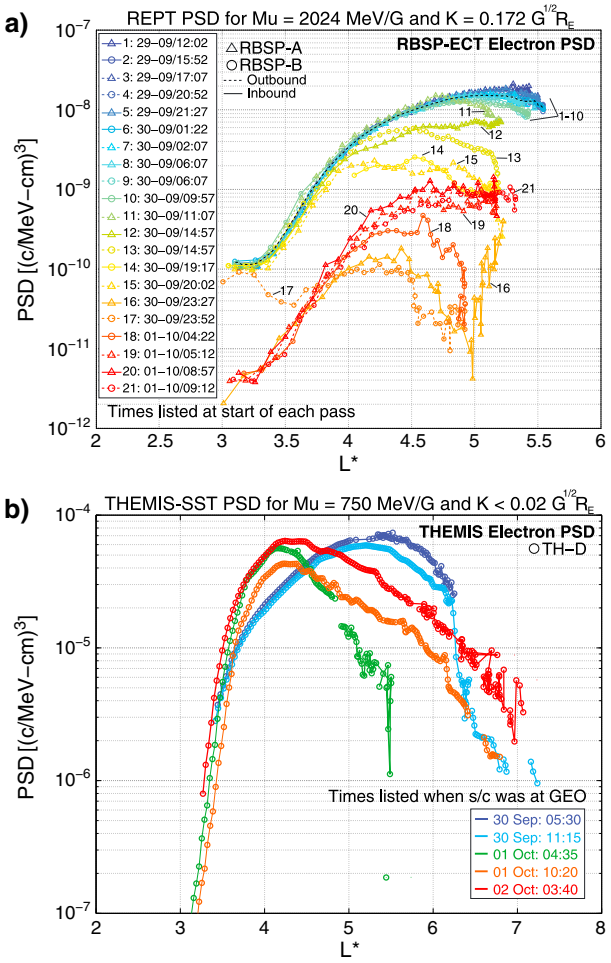

Figure 3. (a) RBSP-ECT REPT electron PSD distributions in L^* for $\mu = 2024$ MeV/G and $K = 0.172\,G^{1/2}\,R_E$. Different colors correspond to different inbound (solid) or outbound (dashed) orbit passes from RBSP-A (triangles) and RBSP-B (circles), with the times labeled for each pass corresponding to the start time of the pass. Each curve has been numbered also for ease of identification. The black dashed line shows the predropout average distribution. (b) THEMIS-D electron PSD distributions in L^* for $\mu = 750$ MeV/G and $K < 0.02\,G^{1/2}\,R_E$. Different passes are shown in different colors with the times for each listed when the spacecraft was at GEO.

dropout is clearly visible in each of the energy channels above 0.22 MeV at the end of the day on 30 September and lasting into 1 October. There were some interesting energy dependencies on the dropout ranges in L and effective duration in time, which are discussed here and also for the recovery of the belt in a companion paper *Turner et al.* [2014]. Here we focus only on the dropout itself, which was broadly effective for relativistic electrons at L shells throughout the majority of the preexisting outer belt.

Figure 3 shows particle distributions in L^* from Van Allen Probes and THEMIS throughout a dropout event from 29 September to 2 October 2012. Starting with electron PSD calculated from the RBSP-ECT REPT instruments (Figure 3a), the preevent distribution showed evidence of a peak between L^* of 5 and 5.5 and was stable during the day leading up to the start of the dropout, as seen from the blue and green curves (i.e., curves 1–10) for the distributions up to 11:07 UT on 30 September and the preevent average distribution shown with the dashed black line. Starting on the outbound RBSP-A distribution from 11:07 UT (i.e., curve 11), the PSD started to drop at $L^* > 5$ (i.e., just after the first solar wind pressure enhancement). On subsequent passes through the belt, this loss of PSD moved from higher L^* to lower as time progressed until the RBSP-A (RBSP-B) outbound (inbound) pass starting at 20:02 (19:17) UT (curves 15 and 14, respectively). When RBSP-A reached apogee around 23:30 UT and then started its inbound trajectory (i.e., curve 16), it observed an abrupt drop in PSD by almost 2 orders of magnitude between L^* of 5.2 and 5 in only ~1.7 h. Meanwhile, RBSP-B was outbound starting at 23:52 UT (curve 17) and observed over an order of magnitude less PSD at $L^* > 3.5$ than it had seen on the previous inbound pass. RBSP-A and RBSP-B were on the same L^* at $L^* \sim 4.5$ during these two passes (i.e., curves 16 for RBSP-A inbound and 17 for RBSP-B outbound), and the time histories of these two distributions revealed that the PSD at $L^* > 4.5$ continued to decrease rapidly after RBSP-A first passed through while at $L^* < 4.5$ the PSD actually increased after RBSP-B first observed it. Then, at $L^* <$ ~3.75, RBSP-A observed over an order of magnitude loss in PSD only ~3.5 h after RBSP-B had observed the same region. On the subsequent passes, both spacecraft observed an increase in PSD at $L^* > 4$ with evidence of a peak in PSD between L^* of 4 and 5 observed by both spacecraft prior to 09:00 UT on 1 October. Note that Figure 3a only shows PSD for one pair of μ and K, but with the REPT instrument, we calculated PSD for ranges of μ from 1000 MeV/G to > 4000 MeV/G and K from $0.015\,G^{1/2}\,R_E$ to $0.387\,G^{1/2}\,R_E$ in the same manner as shown in Figure 3a. Ultimately, the ranges of μ and K examined are limited due to the energy, equatorial pitch angle, and L^* coverage provided by each of the spacecraft. However, note that the data shown in Figure 3, from both THEMIS and the Van Allen Probes,

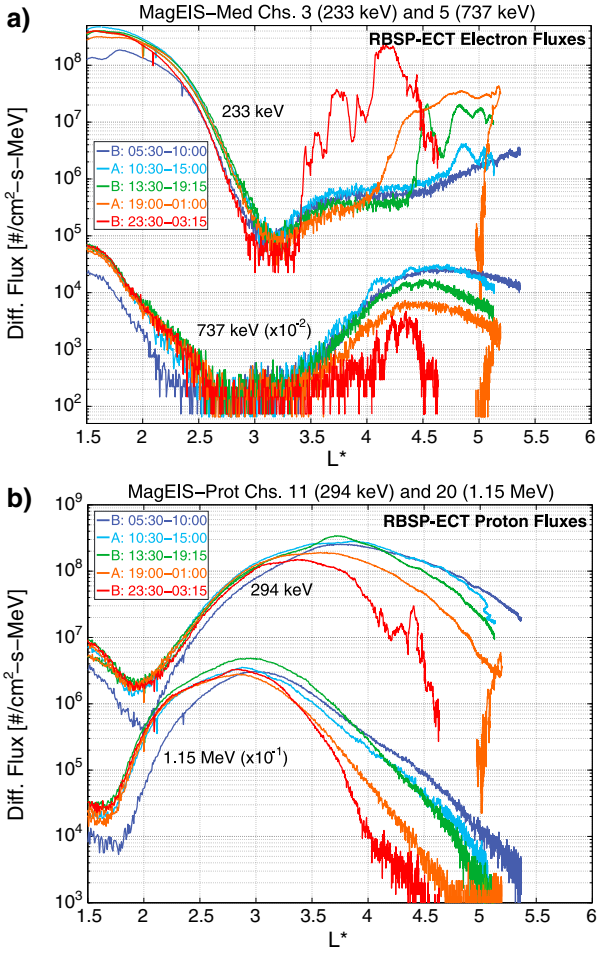

Figure 4. (a) RBSP-ECT MagEIS electron differential flux distributions in L^* from the medium instruments' channels 3 (~233 keV) and 5 (~737 keV). The data have been spin averaged over all look directions and multiplied by 4π sr to produce omnidirectional averages. Different passes are shown in different colors with the time range of each pass listed. The passes all occurred on 30 September, with the exception of the last one shown, which spanned into 1 October. (b) The same as Figure 4a but for MagEIS proton fluxes from channels 11 (~294 keV) and 20 (~1.15 MeV). Note that the MagEIS data inside of $L^* \sim 2.5$ for both electrons and protons are not to be trusted due to high background levels from relativistic protons in the inner belt.

are representative of the results over the full range of relativistic electron μ and K that we were able to examine. These data were used to quantify the extent of the loss during this dropout, which is discussed in the next section.

PSDs from THEMIS were generally consistent with those from the Van Allen Probes for lower μ ($<$ ~1000 MeV/G) and low K ($< 0.02\,G^{1/2}\,R_E$), and the PSD distributions for $\mu = 750$ MeV/G and $K < 0.02\,G^{1/2}\,R_E$ from THEMIS-D (THD) are shown in Figure 3b. Prior to the event (i.e., the 05:30 UT curve), the PSD distribution in L^* was broadly peaked with a peak location at $L^* \sim 5.4$. After passing through GEO at ~11:15 UT, which mapped to $L^* \sim 6.2$ at that time, THD observed a sharp negative gradient in the PSD distribution, in which the PSD fell by an order of magnitude in only $\Delta L^* \approx 0.2$ over ~30 min. Just as was observed by the Van Allen Probes, THEMIS observed the loss in PSD starting at higher L^* and moving to lower L^* over the course of the dropout. On its inbound pass on 1 October, THD was on open drift shells (i.e., undefined L^*) until ~04:30 UT at $L^* \sim 5.5$, consistent with L^*_{max} shown in Figure 1c. On that pass (i.e., the 04:35 UT curve in Figure 3b), THD observed another sharp gradient in the PSD distribution at $L^* \sim 5.4$. At lower L^*, THD revealed a peaked distribution at $L^* \sim 4.2$. On subsequent passes, THD first observed PSD peak reduction at $L^* < 4.5$ and enhanced PSD at $L^* > 4.5$, which combined are evidence of outward radial transport. This was followed by a PSD enhancement that resulted in the peaked distribution shown in the 03:40 UT trajectory. Interestingly, THD did not observe the rapid and extensive loss of PSD at $L^* < 4$ for $\mu \leq 1000$ MeV/G and $K < 0.02\,G^{1/2}\,R_E$ that was observed by the Van Allen Probes at higher μ and K between 23:30 UT on 30 September and 03:30 UT on 1 October. PSD evolution from THA and THE was consistent with that shown here from THD, including details at higher temporal resolution.

The lower energy electron fluxes from the RBSP-ECT MagEIS medium instruments (shown in Figure 4a) revealed the extent of the dropout in electron energy. Like the PSD data from THEMIS and RBSP-ECT REPT, the sharp cutoff in the L^* distribution was also observed in all energies observed by MagEIS (~20 keV to 2 MeV) after the impact of the second solar wind pressure enhancement. However, unlike the relativistic electrons, electrons with energy $<$ ~500 keV showed an increase in flux below L^* of ~4.7, as can be seen from the 233 keV fluxes shown in Figure 4a. Proton data from the MagEIS instruments are shown in Figure 4b, since protons can also provide important information about the dominant loss mechanism during dropouts. These revealed that energetic ring current protons from ~200 keV up to at least 1.15 MeV also experienced a dropout in fluxes during this event with signatures at $L^* > 3.5$ that are remarkably similar to those of the

Table 1. Dropout Timescales (Hours) as a Function of Electron μ, K, and L^* With Respect to the Two Sudden Enhancements in Solar Wind Pressure at 11:30 UT (Top Number) and 23:15 UT (Bottom Number, if Relevant) on 30 September 2012[a]

Mu (MeV/G)	K ($G^{1/2}$ R_E)	$L^*=3$	$L^*=3.5$	$L^*=4.0$	$L^*=4.5$	$L^*=5.0$	$L^*=5.5$	$L^*=6.0$	$L^*=6.5$
500	*< 0.02*	*20.8*	*X*	*X*	*X*	*X*	*17.3*	*< 15.3*	*< 5.0*
		9.0	*X*	*X*	*X*	*X*	*5.5*	*< 3.5*	
750	*< 0.02*	-	*X*	*X*	*X*	*< 19.8*	*< 19.8*	*< 19.8*	*0.5*
			X	*X*	*X*	*< 8.0*	*< 8.0*	*< 8.0*	
1000	*< 0.02*	**X**	*X*	*X*	*X*	*< 19.8*	*< 19.8*	*< 19.8*	*0.5*
		X	*X*	*X*	*X*	*< 8.0*	*< 8.0*	*< 8.0*	
	0.076	**X**	**13.5**	**< 13.5**	-	-	-	-	-
		X	**1.8**	**< 1.8**					
	0.172	**16.3**	**13.5**	**< 13.5**	**10.5**	-	-	-	-
		4.5	**1.8**	**< 1.8**					
	0.387	**< 18.0**	**< 18.0**	**< 13.5**	**10.5**	**6.5**	**< 6.5**	-	-
		< 6.3	**< 6.3**	**< 1.8**					
1423	**< 0.02**	**X**	**X**	**< 14.0**	-	-	-	-	-
		X	**X**	**< 2.3**					
	0.076	**18.0**	**13.5**	**< 13.5**	**< 13.5**	-	-	-	-
		6.3	**1.8**	**< 1.8**	**< 1.8**				
	0.172	**< 16.3**	**13.5**	**< 13.5**	**10.5**	**< 10.5**	-	-	-
		< 4.5	**1.8**	**< 1.8**					
	0.387	-	**13.5**	**< 13.5**	**10.5**	**< 10.5**	**< 6.5**	-	-
			1.8	**< 1.8**					
2024	**< 0.02**	**X**	**< 24.7**	**< 14.0**	-	-	-	-	-
		X	**< 13.0**	**< 2.3**					
	0.076	**< 18.0**	**13.5**	**< 13.5**	**< 13.5**	**9.0**	-	-	-
		< 6.3	**1.8**	**< 1.8**	**< 1.8**				
	0.172	**< 16.3**	**13.5**	**< 13.5**	**10.5**	**< 9.0**	-	-	-
		< 4.5	**1.8**	**< 1.8**					
	0.387	-	-	**< 13.5**	**10.5**	**< 10.5**	**< 10.5**	-	-
				< 1.8					
2879	**< 0.02**	**< 24.7**	**< 24.7**	**< 14.0**	**< 14.0**	**< 14.0**	-	-	-
		< 13.0	**< 13.0**	**< 2.3**	**< 2.3**	**< 2.3**			
	0.076	**< 18.0**	**13.5**	**< 13.5**	**< 13.5**	**11.3**	**< 7.8**	-	-
		< 6.3	**1.8**	**< 1.8**	**< 1.8**				
	0.172	-	**13.5**	**< 13.5**	**< 13.5**	**10.5**	**< 7.8**	-	-
			1.8	**< 1.8**	**< 1.8**				
	0.387	-	-	-	**10.5**	**10.5**	**5.3**	-	-
4095	**< 0.02**	**< 24.7**	**< 24.7**	**< 14.0**	**< 14.0**	**< 14.0**	-	-	-
		< 13.0	**< 13.0**	**< 2.3**	**< 2.3**	**< 2.3**			
	0.076	-	**13.5**	**< 13.5**	**< 13.5**	**11.3**	**< 7.8**	-	-
			1.8	**< 1.8**	**< 1.8**				
	0.172	-	-	**< 13.5**	**< 13.5**	**10.5**	**< 7.8**	-	-
				< 1.8	**< 1.8**				
	0.387	-	-	-	-	-	-	-	-

[a]Times are calculated by when the PSD dropped by $1/e^2$ (~86%) of the preevent average at those coordinates. Results from THEMIS are in italics and Van Allen Probes in bold. "X" implies that the PSD did not drop out below $1/e^2$, and "-" indicates insufficient data. The "< t" indicates that the loss at that L^* occurred before the measurement was made at time "t"; how long before depended on the satellites' revisit times in L^*.

relativistic electrons. From Figures 4a and 4b, it is clear that electrons above ~500 keV and 100 s keV to ~1 MeV protons behaved similar to the electrons observed by RBSP-ECT REPT and THEMIS, that is, the dropout started at higher L^* and moved in, there was a sharp cutoff in the distribution between L^* of 5 and 5.5 after 23:30 UT on 30 September, and there was evidence of enhancements in 100 s of keV electron fluxes at $3.5 < L^* < 4.5$ in the early hours of 1 October.

3. Results: Quantifying Dropout Timescales and Effective Ranges

From the PSD data presented in the previous section, we quantified dropout e^2-folding timescales (corresponding to ~86% loss) for relativistic electrons as a function of μ, K, and L^*. The results are shown in Table 1. These timescales revealed that the loss was generally dependent on all three adiabatic invariants. The

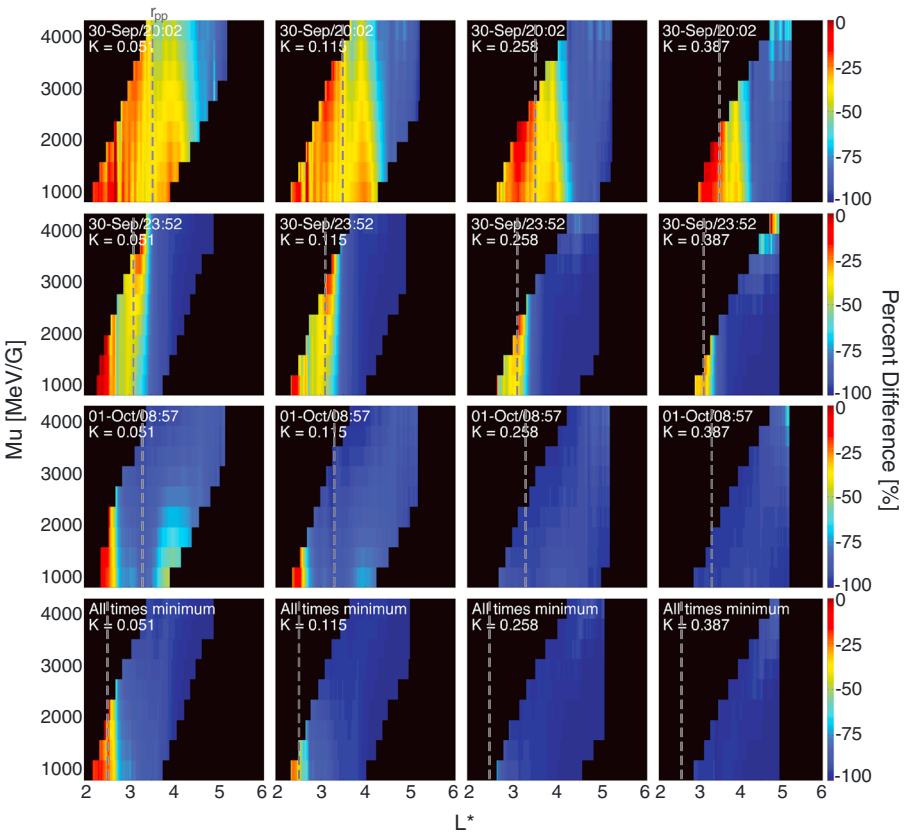

Figure 5. Percent loss of electron PSD as a function of μ, K, and L^* and time compared to the preevent average distributions from the RBSP-ECT REPT instruments. Each of the top three rows corresponds to a different pass time (20:02, 23:52, and 08:57 UT from top down), while the different columns correspond to different values of K (0.051, 0.115, 0.258, and 0.387 $G^{1/2} R_E$, respectively, from left to right). The dashed gray lines indicate the plasmapause location (r_{pp}, in radial distance with units of R_E) observed by the Van Allen Probes during each pass. The bottom row shows the minimum percent difference from all times after the start of the dropout in the same format as the upper rows. The plasmapause location in the bottom row was the innermost location observed by the Van Allen Probes during the dropout (see Table 2).

fastest losses occurred at higher L^*s, and the timescales increased for lower L^*s (clear in the Van Allen Probes timescales, though note that the THEMIS timescales are limited by the long orbital periods of those spacecraft). The only range examined that did not fall below $1/e^2$ of the preevent average was that of electrons at low L^*, low μ, and the lowest Ks examined (e.g., $\mu = 500$ MeV/G, $K < 0.02\ G^{1/2} R_E$ at $3.5 < L^* < 5$ and $\mu = 2024$ MeV/G, $K < 0.02\ G^{1/2} R_E$ at $L^* = 3$ only). At $L^* \geq 4$, the dropout caused more than 86% loss in less than 14 h after the impact of the first solar wind pressure enhancement, with timescales that were fastest at higher L^*s and slowest at $L^* = 4$ but relatively independent of μ and K (except for $\mu \leq 1000$ MeV/G and $K < 0.02\ G^{1/2} R_E$, where the PSD never dropped by $1/e^2$ with the exception of $\mu = 500$ MeV/G at $L^* = 3$). However, the PSD losses at $L^* < 4$ were highly dependent on μ and K, with losses occurring faster for high μ, high K electrons. The loss of PSD for $\mu = 500$ MeV/G at $L^* = 3$ was likely due to slow, energy-dependent decay from interactions with plasmaspheric hiss [e.g., *Thorne et al.*, 2013].

Comparing PSDs from REPT on each pass after the dropout started around 11:30 UT on 30 September to the preevent average distributions (as shown in Figure 3a), we calculated the percent loss as a function of μ, K, L^*, and time. The results from this analysis are summarized with the plots shown in Figure 5. Starting with the top row of plots in Figure 5, which correspond to the percent loss throughout the outer belt by the 20:02 UT outbound trajectory of RBSP-A, it is clear that the loss of PSD above L^* of 4.5 for all μ and K shown was $> 80\%$ of the preevent average, with stronger losses at higher L^*s. However, there is a K dependence on the results: the loss extended to lower L^* for higher Ks. There was also evidence of a peak in PSD at $3.5 < L^* < 4.5$, just outside of the plasmapause (r_{pp}), which was most distinct at the lowest μ and K examined. We determined r_{pp}

Table 2. Location of the Plasmapause in Radial Distance and MLT as Observed by the Van Allen Probes Throughout the Event[a]

Observation Time (MM-DD/hh:mm)	RBSP-A or RBSP-B	Plasmapause Radial Distance (R_E)	Observation MLT
9-30/16:10 UT	B	4.1	~05:00
9-30/21:00 UT	A	3.5	~04:00
10-1/00:30 UT	B	3.1	~03:30
10-1/03:45 UT	A	3.0	~11:20
10-1/05:15 UT	A	2.5	~02:30
10-1/07:30 UT	B	3.3	~10:00

[a]These plasmapause locations were calculated based on the Electric and Magnetic Field Instrument Suite and Integrated Science (EMFISIS) upper hybrid line. The spacecraft used to make each observation is indicated in the second column, and the radial distance and MLT at which each observation was made are listed in the third and fourth columns, respectively. The plasmapause was compressed to ~2.5 R_E at ~10-1/05:15 UT, which is roughly consistent with the electron loss observed down to L^* of ~2.6 by REPT. In other words, the significant loss occurred down to the location very close to the innermost extent of the plasmapause.

for this study using Van Allen Probes wave data, and the locations for each Van Allen Probes pass through it are shown in Table 2. Inside of the plasmapause, the loss was considerably lower at all μ and K. This period corresponds to our best estimates of the extent of the loss after the start of the dropout following the first sudden enhancement of solar wind dynamic pressure.

The second and third rows of plots shown in Figure 5 demonstrate the evolution and extent of the loss after the second enhancement of solar wind pressure. From the 23:52 UT results, the extensive loss extended into $L^* \sim 3.5$ for all μ and K, but inside of $L^* \sim 3.5$, the amount lost was greater for lower μ than for higher. Note that the data at highest μ and K were near background levels, explaining the increased noise (and thus discrepancy) in the results there. By 08:57 UT on 1 October, the outer belt had been essentially entirely wiped out at $L^* > 2.75$, except for evidence of a peak in PSD starting to form at $3.5 < L^* < 4.5$. Consistent with the previous evidence of a peak, the peak was strongest at lowest μ and K and appeared outside of the plasmapause. The bottom row of Figure 5 shows the minimum PSD from all times after the second part of the dropout started as a function of μ, K, and L^*. These plots reveal the maximum extent of the loss observed during this dropout. Ultimately, even more PSD was lost in the heart of the belt, since the PSD peaks indicate a competing source process was active during the dropout itself. From these plots, it is clear that at $L^* > 2.75$, which notably corresponds to all L^* outside of the minimum plasmapause location as observed by the Van Allen Probes, the dropout was > ~90% for all the electrons observed by RBSP-ECT REPT.

4. Discussion

Based on the evidence shown in the previous sections, we examined which loss mechanism could result in such rapid loss over extensive ranges of electron energy (and μ), equatorial pitch angle (and K), and L^* and for different species. Wave-particle interactions with EMIC waves would have been most effective for electrons at higher energies and equatorial pitch angles nearest the loss cone; EMIC waves would likely have been entirely ineffective for electrons with energies below ~500 keV and at certain L^*s [e.g., *Meredith et al.*, 2003; *Shprits et al.*, 2008; *Ukhorskiy et al.*, 2010]. However, the observed features are all entirely consistent with magnetopause shadowing and subsequent enhanced outward radial transport. The dropout started immediately after the impact of the first sudden enhancement of solar wind dynamic pressure. Loss started at higher L^* and moved inward in time (see Figure 3), and THEMIS observed a sharp, negative gradient in the PSD L^* distribution at $L^* \sim 6.4$, which is necessary to propagate the losses to lower L^*s [e.g., *Shprits et al.*, 2006; *Turner et al.*, 2012a, 2012b], which was also observed here. This cutoff in the distribution also corresponds to L^*_{max} after the first solar wind pressure enhancement (Figure 1c). After the second solar wind pressure enhancement, the dropout extended rapidly to lower L^*s (see Figure 3). A sharp cutoff in the PSD and flux distributions was observed again by both the Van Allen Probes and THEMIS at $5 < L^* < 5.5$ for electrons and protons, a location consistent with the L^*_{max} from the TS05 model (Figure 1c). RBSP-A was inbound immediately after the second pressure enhancement (~23:30 UT; compare Figures 1a and 1c and curve 16 in Figure 3a) when it observed the sharp cutoff in the PSD distribution, which was actually a rapid, temporal decrease in PSD around $L^* \sim 5$; we interpret this as a direct observation of the rapid loss of PSD due to rapid outward transport very near the last closed drift shell boundary following magnetopause shadowing. At

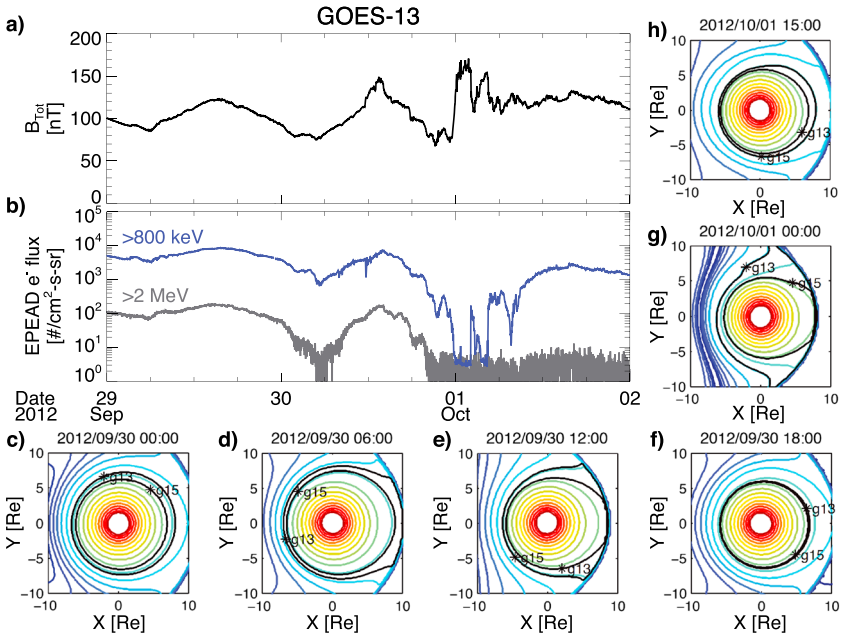

Figure 6. GOES-13 data and TS05 mapping during the event. (a,b) GOES-13 magnetic field strength and Energetic Proton, Electron and Alpha Detectors (EPEAD) fluxes of >800 keV and >2 MeV electrons from 29 September to 2 October 2012. (c–h) Contours of constant magnetic field in the magnetic equatorial plane, corresponding to drift shells for equatorially mirroring particles, calculated using the TS05 model for six different times during the period 00:00, 06:00, 12:00, and 18:00 UT on 30 September and 00:00 and 15:00 UT on 1 October. The locations of GOES-13 and GOES-15 are indicated with asterisks, and their corresponding drift shells are marked in black. The other drift shells are color coded based on the magnetic field strength. This clearly shows when GOES spacecraft mapped onto drift trajectories that intersected the magnetopause and the two magnetopause shadowing events starting around 11:00 UT on 30 September and 00:00 UT on 1 October. These also explain the drop in fluxes observed by GOES-13 around 06:00 UT on the thirtieth, when the spacecraft mapped onto open drift trajectories when it was near midnight Magnetic Local Time (MLT).

$L^* >$ ~3.5, the Van Allen Probes also observed a dropout in ~200 keV to >1 MeV protons, which also started at higher L^* and moved in to lower L^* over several hours and revealed a sharp cutoff in the L^* distribution after the second solar wind pressure enhancement. The close to 2 orders of magnitude or more drop in the proton fluxes at higher L^* was more than that expected from adiabatic variations alone [e.g., *Kim and Chan*, 1997]. We also investigated the equatorial pitch angle distributions for these protons throughout the dropout and confirmed that the drop in flux was not simply the result of the spacecraft observing different ranges of a very steep equatorial pitch angle distribution. Thus, we interpret the observed drop in proton flux at $L^* >$ ~3.5 as being predominant from actual losses from the system. This loss of energetic protons is a critical observation supporting our conclusion, since magnetopause shadowing and enhanced outward radial transport should also occur for energetic ring current ions [e.g., *Green et al.*, 2004]; however, it is important to examine ions at energies above those typically injected into the inner magnetosphere from the plasma sheet during active times (i.e., > a few 100 keV), as we have done here. GOES data and drift shell modeling in the TS05 model also confirmed this two-part dropout, with clear signatures of magnetopause shadowing in >0.8 MeV and >2.0 MeV electron fluxes, corresponding to the impacts of the two enhancements in solar wind dynamic pressure. These results are summarized in Figure 6.

The plasmapause appears to have played a critical role in limiting the extent of the dropout. From the Van Allen Probes observations (see Figure 5), the most amount of PSD loss occurred outside of the plasmapause throughout the event. Inside of the minimum plasmapause location during the event, the loss of PSD was very small, only ~20% or less. We suggest that this may be the result of the plasmasphere shielding the trapped electrons within it by damping ULF wave amplitudes [e.g., *Hartinger et al.*, 2012, and references therein], significantly limiting the effect of those waves on the radial transport of electrons. Essentially, the cascade of outward radial transport that can follow magnetopause shadowing is enabled by ULF wave activity, since these waves result in radial transport of trapped particles [e.g., *Ukhorskiy et al.*, 2009], but if those waves cannot penetrate

the plasmasphere, then the diffusion should not be as rapid there. Also, the plasmapause erodes to much lower L shells during active periods [e.g., *Goldstein et al*., 2003], meaning the diffusion rate is still very slow compared to at higher L shells. Furthermore, other loss and source mechanisms resulting from wave-particle interactions with EMIC and chorus waves should occur primarily outside of the plasmapause [e.g., *Meredith et al*., 2003; *Santolik et al*., 2003], which should further limit most of the dynamics to the region outside of the plasmapause.

A dropout resulting from magnetopause shadowing and outward transport should result in an enhancement of PSD at L^* inside of ~4 [e.g., *Turner et al*., 2012a, 2012b]. That was observed by THEMIS for electrons at $\mu \leq$ ~1000 MeV/G and $K \sim 0\,G^{1/2}\,R_E$ (e.g., Figure 3b) and, interestingly, also for the protons from Van Allen Probes (e.g., Figure 4b), but not for electrons at higher μ and K observed by the Van Allen Probes (e.g., Figure 3a) during this event. The sudden loss observed at $L^* <$ ~3.75 after ~23:30 UT on 30 September by the Van Allen Probes must have resulted from some other loss mechanism, potentially from scattering by EMIC waves based on the fact that the loss occurred outside of the plasmapause in only a few hours, was only evident in the PSD for multi-MeV electrons, and was strongest at higher K. This event was also one of three simulated recently by *Hudson et al*. [2014], who came to one of the same conclusions as we reach here: two different loss mechanisms can operate over different ranges of L shells during dropout events. Additionally, there was strong evidence of a local source of PSD effective outside of the plasmapause ongoing and competing with the loss throughout the entirety of this dropout. This source was strongest at lowest μ and K and occurred where injections in 10 s–100 s of keV electrons were clear from the MagEIS fluxes (e.g., 233 keV flux in Figure 4a), which is consistent with local acceleration by whistler mode chorus waves [e.g., *Reeves et al*., 2013]. These features are of extreme interest and are the topic of another study, *Turner et al*. [2014].

5. Conclusions

Examining the unprecedented level of data coverage from the Van Allen Probes, THEMIS, and GOES during the 30 September 2012 dropout event led us to the following conclusions:

1. At $L^* >$ ~4, the dropout was highly consistent with loss due to magnetopause shadowing and subsequent rapid outward radial transport, and this loss mechanism is also effective for energetic ring current protons (100 s of keV to > 1 MeV).
2. The rapid loss of preferentially high μ, high K electrons observed at $L^* <$ ~4 cannot be explained by magnetopause shadowing; we speculate that this loss resulted from rapid scattering into the atmospheric loss cone due to wave-particle interactions. This indicates that two different loss mechanisms can contribute at equal levels at different L^*s during a dropout, with losses at $L^* >$ ~4 dominated by magnetopause shadowing and outward transport and losses at lower L^* dominated by wave-particle interactions. This is the same as the concept proposed by *Bortnik et al*. [2006] and is also consistent with the simulations of a dropout on 2 Sep. 2012 by *Shprits et al*. [2013], who showcased the important energy dependencies of different outer belt acceleration and loss mechanisms.
3. Dropouts can result in rapid (< ~1/2 day) loss of > ~90% of the preevent population over the full extent of the outer belt, from 100 s of keV to multi-MeV (and μ from a few 100 s of MeV/G to > 4000 MeV/G), the full range of equatorial pitch angles (and K from < 0.02 to > $0.4\,G^{1/2}\,R_E$), and all $L^* \geq$ ~3. This demonstrates that dropouts can serve very effectively as a "hard reset" on the outer belt system and any subsequent enhancements are a new population of electrons from some source, which, as was the case here, may be active during the dropout itself.

Acknowledgments

We are thankful to the THEMIS and Van Allen Probes missions, NASA's CDAWeb, OMNI, and NOAA's GOES and NGDC for online data access and data analysis tools. RBSP-ECT work was supported under NASA prime contract NAS5-01072 to Johns Hopkins University Applied Physics Laboratory (JHU/APL). Work at LANL was performed under the auspices of the United States Department of Energy. D.L. Turner is thankful for funding from NASA's THEMIS mission (contract NAS5-02099), a NASA grant (NNX12AJ55G), and the Monitoring, Analyzing, and Assessing the Radiation Belt Loss and Energization (MAARBLE) project funded under the European Commission's (EC) FP7 framework (Note that this work reflects the authors' views, and the EC is not liable for any use that may be made of the information contained herein).

Robert Lysak thanks the reviewers for their assistance in evaluating this paper.

References

Angelopoulos, V. (2008), The THEMIS Mission, *Space Sci. Rev.*, *141*, 5–34, doi:10.1007/s11214-008-9336-1.

Baker, D. N., et al. (2012), The Relativistic Electron-Proton Telescope (REPT) instrument on board the Radiation Belt Storm Probes (RBSP) spacecraft: Characterization of Earth's radiation belt high-energy particle populations, *Space Sci. Rev.*, *179*, 337–381, doi:10.1007/s11214-012-9950-9.

Baker, D. N., et al. (2013), A long-lived relativistic electron storage ring embedded in Earth's outer Van Allen belt, *Science*, *340*, 186–190, doi:10.1126/science.1233518.

Blake, J. B., et al. (2013), The Magnetic Electron Ion Spectrometer (MagEIS) instruments aboard the Radiation Belt Storm Probes (RBSP) spacecraft, *Space Sci. Rev.*, *179*, 383–421, doi:10.1007/s11214-013-9991-8.

Borovsky, J. E., and M. Denton (2009), Relativistic-electron dropouts and recovery: A superposed epoch study of the magnetosphere and solar wind, *J. Geophys. Res.*, *114*, A02201, doi:10.1029/2008JA013128.

Bortnik, J., R. M. Thorne, T. P. O'Brien, J. C. Green, R. J. Strangeway, Y. Y. Shprits, and D. N. Baker (2006), Observation of two distinct, rapid loss mechanisms during the 20 November 2003 radiation belt dropout event, *J. Geophys. Res.*, *111*, A12216, doi:10.1029/2006JA011802.

Dessler, A. J., and R. Karplus (1961), Some effects of diamagnetic ring currents on Van Allen radiation, *J. Geophys. Res.*, *66*(8), 2289–2295.
Goldstein, J., B. R. Sandel, W. T. Forrester, and P. H. Reiff (2003), IMF-driven plasmasphere erosion of 10 July 2000, *Geophys. Res. Lett.*, *30*(3), 1146, doi:10.1029/2002GL016478.
Green, J. C., T. G. Onsager, T. P. O'Brien, and D. N. Baker (2004), Testing loss mechanisms capable of rapidly depleting relativistic electron flux in the Earth's outer radiation belt, *J. Geophys. Res.*, *109*, A12211, doi:10.1029/2004JA010579.
Hartinger, M., V. Angelopoulos, M. B. Moldwin, Y. Nishimura, D. L. Turner, K.-H. Glassmeier, M. G. Kivelson, J. Matzka, and C. Stolle (2012), Observations of a Pc5 global (cavity/waveguide) mode outside the plasmasphere by THEMIS, *J. Geophys. Res.*, *117*, A06202, doi:10.1029/2011JA017266.
Hudson, M. K., D. N. Baker, J. Goldstein, B. T. Kress, J. Paral, F. R. Toffoletto, and M. Wiltberger (2014), Simulated magnetopause losses and Van Allen Probe flux dropouts, *Geophys. Res. Lett.*, *41*, doi:10.1002/2014GL059222.
Kilpua, E. K. J., A. Isavnin, A. Vourlidas, H. E. J. Koskinen, and L. Rodriguez (2013), On the relationship between interplanetary coronal mass ejections and magnetic clouds, *Ann. Geophys.*, *31*, 1251–1265, doi:10.5194/angeo-31-1251-2013.
Kim, H.-J., and A. A. Chan (1997), Fully adiabatic changes in storm time relativistic electron fluxes, *J. Geophys. Res.*, *102*(A10), 22,107–22,116.
Kim, K. C., D.-Y. Lee, H.-J. Kim, L. R. Lyons, E. S. Lee, M. K. Ozturk, and C. R. Choi (2008), Numerical calculations of relativistic electron drift loss effect, *J. Geophys. Res.*, *113*, A09212, doi:10.1029/2007JA013011.
Koller, J., and S. Zaharia (2011), LANL* V2.0: Global modeling and validation, *Geosci. Model Dev.*, *4*, 669–675.
Li, X., D. N. Baker, M. Temerin, T. E. Cayton, E. G. D. Reeves, R. A. Christensen, J. B. Blake, M. D. Looper, R. Nakamura, and S. G. Kanekal (1997), Multisatellite observations of the outer zone electron variation during the November 3–4, 1993 magnetic storm, *J. Geophys. Res.*, *102*(A7), 14,123–14,140.
Lin, R. L., X. X. Zhang, S. Q. Liu, Y. L. Wang, and J. C. Gong (2010), A three-dimensional asymmetric magnetopause model, *J. Geophys. Res.*, *115*, A04207, doi:10.1029/2009JA014235.
Loto'aniu, T. M., H. J. Singer, C. L. Waters, V. Angelopoulos, I. R. Mann, S. R. Elkington, and J. W. Bonnell (2010), Relativistic electron loss due to ultralow frequency waves and enhanced outward radial diffusion, *J. Geophys. Res.*, *115*, A12245, doi:10.1029/2010JA015755.
Mauk, B. H., N. J. Fox, S. G. Kanekal, R. L. Kessel, D. G. Sibeck, and A. Ukhorskiy (2012), Science objectives and rationale for the Radiation Belt Storm Probes mission, *Space Sci. Rev.*, *179*, 3–27, doi:10.1007/s11214-012-9908-y.
Meredith, N. P., R. M. Thorne, R. B. Horne, D. Summers, B. J. Fraser, and R. R. Anderson (2003), Statistical analysis of relativistic electron energies for cyclotron resonance with EMIC waves observed on CRRES, *J. Geophys. Res.*, *108*(A6), 1250, doi:10.1029/2002JA009700.
Miyoshi, Y., V. K. Jordanova, A. Morioka, M. F. Thomsen, G. D. Reeves, D. S. Evans, and J. C. Green (2006), Observations and modeling of energetic electron dynamics during the October 2001 storm, *J. Geophys. Res.*, *111*, A11S02, doi:10.1029/2005JA011351.
Morley, S. K., R. H. W. Friedel, E. L. Spanswick, G. D. Reeves, J. T. Steinberg, J. Koller, T. E. Cayton, and E. Noveroske (2010), Dropouts of the outer electron radiation belt in response to solar wind stream interfaces: Global positioning system observations, *Proc. Roy. Soc. A*, *466*, 3329–3350, doi:10.1098/rspa.2010.0078.
Morley, S. K., M. G. Henderson, G. D. Reeves, and R. H. W. Friedel (2013), Phase space density matching of relativistic electrons using the Van Allen Probes: REPT results, *Geophys. Res. Lett.*, *40*, 4798–4802, doi:10.1002/grl.50909.
Reeves, G. D., et al. (2013), Electron acceleration in the heart of the Van Allen radiation belts, *Science*, *341*(6149), 991–994, doi:10.1126/science.1237743.
Roederer, J. G. (1970), *Dynamics of Geomagnetically Trapped Radiation*, Springer, New York.
Santolik, O., D. A. Gurnett, J. S. Pickett, M. Parrot, and N. Cornilleau-Wehrlin (2003), Spatio-temporal structure of storm-time chorus, *J. Geophys. Res.*, *108*(A7), 1278, doi:10.1029/2002JA009791.
Shprits, Y. Y., R. M. Thorne, R. H. W. Friedel, G. D. Reeves, J. Fennell, D. N. Baker, and S. G. Kanekal (2006), Radial diffusion driven by losses at magnetopause, *J. Geophys. Res.*, *111*, A11214, doi:10.1029/2006JA011657.
Shprits, Y. Y., D. A. Subbotin, N. P. Meredith, and S. Elkington (2008), Review of modeling of losses and sources of relativistic electrons in the outer radiation belt II: Local acceleration and loss, *J. Atmos. Sol. Terr. Phys.*, *70*, 1694–1713, doi:10.1016/j.jastp.2008.06.014.
Shprits, Y. Y., D. Subbotin, A. Drozdov, M. E. Usanova, A. Kellerman, K. Orlova, D. N. Baker, D. L. Turner, and K.-C. Kim (2013), Unusual stable trapping of the ultrarelativistic electrons in the Van Allen radiation belts, *Nat. Phys.*, *9*, 699–703, doi:10.1038/NPHYS2760.
Spence, H. E., et al. (2013), Science goals and overview of the energetic particle, composition, and thermal plasma (ECT) suite on NASA's Radiation Belt Storm Probes (RBSP) mission, *Space Sci. Rev.*, *179*, 311–336, doi:10.1007/s11214-013-0007-5.
Summers, D., and R. M. Thorne (2003), Relativistic electron pitch-angle scattering by electromagnetic ion cyclotron waves during geomagnetic storms, *J. Geophys. Res.*, *108*(A4), 1143, doi:10.1029/2002JA009489.
Tao, X., J. Bortnik, R. M. Thorne, J. M. Albert, and W. Li (2012), Effects of amplitude modulation on nonlinear interactions between electrons and chorus waves, *Geophys. Res. Lett.*, *39*, L06102, doi:10.1029/2012GL051202.
Thorne, R. M., et al. (2013), Evolution and slow decay of an unusual narrow ring of relativistic electrons near L~3.2 following the September 2012 magnetic storm, *Geophys. Res. Lett.*, *40*, 3507–3511, doi:10.1002/grl.50627.
Tsyganenko, N. A., and M. I. Sitnov (2005), Modeling the dynamics of the inner magnetosphere during strong geomagnetic storms, *J. Geophys. Res.*, *110*, A03208, doi:10.1029/2004JA010798.
Turner, D. L., Y. Y. Shprits, M. Hartinger, and V. Angelopoulos (2012a), Explaining sudden losses of outer radiation belt electrons during geomagnetic storms, *Nat. Phys.*, *8*, 208–212, doi:10.1038/NPHYS2185.
Turner, D. L., S. K. Morley, Y. Miyoshi, B. Ni, and C.-L. Huang (2012b), *Outer Radiation Belt Flux Dropouts: Current Understanding and Unresolved Questions*, Geophysical Monograph Series, vol. 199, edited by D. Summers, I. R. Mann, and D. N. Baker, pp. 195-212, AGU, Washington, D. C., doi:10.1029/2012GM001310.
Turner, D. L., V. Angelopoulos, Y. Shprits, A. Kellerman, P. Cruce, and D. Larson (2012c), Radial distributions of equatorial phase space density for outer radiation belt electrons, *Geophys. Res. Lett.*, *39*, L09101, doi:10.1029/2012GL051722.
Turner, D. L., V. Angelopoulos, W. Li, M. D. Hartinger, M. Usanova, I. R. Mann, J. Bortnik, and Y. Shprits (2013), On the storm-time evolution of relativistic electron phase space density in Earth's outer radiation belt, *J. Geophys. Res. Space Physics*, *118*, 2196–2212, doi:10.1002/jgra.50151.
Turner, D. L., et al. (2014), Competing source and loss mechanisms due to wave-particle interactions in Earth's outer radiation belt during the 30 September to 2 October 2012 geomagnetic storm, *J. Geophys. Res. Space Physics*, doi:10.1002/2014JA019770, in press.
Ukhorskiy, A. Y., M. I. Sitnov, K. Takahashi, and B. J. Anderson (2009), Radial transport of radiation belt electron due to stormtime Pc5 waves, *Ann. Geophys.*, *27*, 2173–2181.
Ukhorskiy, A. Y., Y. Y. Shprits, B. J. Anderson, K. Takahashi, and R. M. Thorne (2010), Rapid scattering of radiation belt electrons by storm-time EMIC waves, *Geophys. Res. Lett.*, *37*, L09101, doi:10.1029/2010GL042906.